Optical spectra of PbTe/$Pb_{1-x}Eu_xTe$ quantum wells

E. Abramof, E. A. de Andrada e Silva, S. O. Ferreira,* P. Motisuke, P. H. O. Rappl, and A. Y. Ueta
Laboratório Associado de Sensores e Materiais - LAS, Instituto Nacional de Pesquisas Espaciais - INPE, C.P. 515, 12201-970 São José dos Campos - SP, Brazil
(Received 17 July 2000; published 1 February 2001)

The optical absorption spectrum of PbTe quantum wells is revisited. A series of PbTe/$Pb_{1-x}Eu_xTe$ multiple quantum well (MQW) samples with x between 0.05 and 0.07 was grown by molecular-beam epitaxy on (111)BaF_2 substrates. The PbTe well width was varied from 2.3 to 20.6 nm, while the barrier was kept thicker than 44.2 nm. The transmission spectra were measured at varying temperature (5–300 K) and the energy of the different optical transitions between quantized electron and hole states was obtained from the corresponding absorption steps. Several transitions, from both longitudinal and oblique valleys, are clearly observed. Contrary to what is commonly believed, an overall agreement (i.e., for different transitions, temperatures, and PbTe well widths) is found between the experimental results and the electric-dipole optical transition energies calculated analytically, within the envelope function approximation and the perfect square well model. The effects of the strain inside the thin PbTe layers on the optical transition energies are included in the calculations and studied as a function of well width and temperature. The amount of tensile strain was measured with high-resolution x-ray diffraction at room temperature. From the fit to the experiment, we evaluate the PbTe deformation potentials. At low temperatures, a blueshift is observed in the energy of the longitudinal transitions of the narrow wells, which is attributed to the mismatch in the thermal expansion coefficient between the MQW structure and the BaF_2 substrate.

DOI: 10.1103/PhysRevB.63.085304 PACS number(s): 78.66.Li, 73.22.−b, 61.10.−i

I. INTRODUCTION

With the addition of a few percent of Eu, the energy gap of the ternary $Pb_{1-x}Eu_xTe$ is considerably increased with respect to that of the pure PbTe, while its rocksalt structure remains the same, except for a slight increase in the lattice constant. These properties make $Pb_{1-x}Eu_xTe$ a suitable and important barrier material to use, for instance, in the study of quantum confinement effects in (strained) PbTe quantum wells (QW's). These structures are of interest in the physics of new semiconductor devices for both their spectral range and the peculiar electronic properties of the IV-VI semiconductor compounds. The large confinement obtained with such high barriers has already contributed to the improvement of PbTe QW infrared lasers.[1,2]

More recently, the properties of different PbTe quantum structures have attracted much attention. It is worth mentioning, for example, the studies of quantum dot superlattices,[3] conductance quantization in small constrictions,[4] and enhanced thermoelectric power in [111] PbTe QW's.[5] Compared to the more studied III-V or II-VI semiconductor QW's, the physics of IV-VI QW's is more complex, for instance, due to the difficulties in the infrared optics and to the presence of anisotropic and nonparabolic multiple valleys.

In particular, the studies of the PbTe QW optical transmission spectrum, which is a direct probe of quantum effects, have been limited to few samples and fixed temperatures. Ishida *et al.*[6] have reported on the optical spectra measured at room temperature, with a series of [100] PbTe/$Pb_{0.95}Eu_{0.05}Te$ QW's. The spectra of [111] PbTe/$Pb_{1-x}Eu_xTe$ QW's was investigated in detail by Yuan *et al.*[7] However, only three samples were used, with $x = 0.026$, 0.03, and 0.024, respectively, and the transmission measurements were done at 77 and 5 K. Sophisticated modeling,[8,9] with long numerical calculations, was used in both studies. In this paper, the optical spectra of the PbTe QW's is readdressed. For this purpose, a series of PbTe/$Pb_{1-x}Eu_xTe$ multiple quantum well (MQW) samples was grown by molecular-beam epitaxy on (111)BaF_2 substrates. Compared to the series of samples used in the previous studies,[6,7] the present series spans a larger range of PbTe well width (from 2.3 to 20.6 nm) and presents higher Eu concentrations ($0.05 < x < 0.07$) and therefore higher potential barriers and stronger quantum confinement. The transmission spectra were measured at several temperatures between 5 and 300 K and the subband to subband transition energies were obtained from the corresponding absorption steps. Several transitions, involving both longitudinal and oblique valleys, were clearly observed. Contrary to what is commonly believed, an overall good agreement is found between the experimental results and the electric-dipole optical transition energies calculated analytically within the envelope-function approximation and the perfect square well model.

The good agreement is only obtained when considering carefully the strain effects. We have determined the tensile parallel strain inside the PbTe layer, for all MQW samples, with high-resolution x-ray diffraction analysis at room temperature. As for the theory, we have extended the envelope-function model proposed in Ref. 10, in order to include the strain corrections. The comparison between experimental and theoretical results for different transitions, as a function of well width and temperature, allowed us not only to testify for the reliability of both theoretical and experimental methods, but also to further study the deformation effects.

From the best fit to the experiment, we have evaluated the PbTe deformation potentials. Among the controversial values found in the literature, good agreement is obtained with

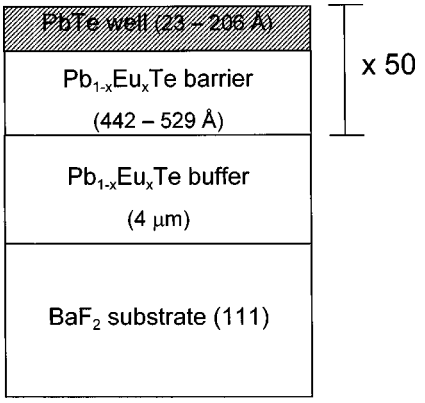

FIG. 1. Schematic diagram of the structure of the $PbTe/Pb_{1-x}Eu_xTe$ MQW samples grown by MBE and used here in the investigation of the PbTe QW transmission spectra.

those determined from luminescence measurements[11,12] and first-principles calculations.[13] It was also found that, when lowering the temperature, all transition energies decrease almost parallel to the PbTe band gap down to near 100 K. Below 100 K however, the transitions from the longitudinal valley in the narrow wells reach a minimum and start increasing. This can be explained with the buildup of further tensile strain in the thin PbTe layers, due to the difference between the thermal expansion coefficients of the MQW structure and the BaF_2 substrate.[14]

The rest of this paper is divided into the following sections: Sec. II, with the details of the molecular-beam epitaxy (MBE) growth and structural characterization of the $PbTe/Pb_{1-x}Eu_xTe$ MQW samples; Sec. III, where we describe the measurement and the analysis of the optical transmission spectra; Sec. IV, which presents the theoretical model, including the strain corrections; Sec. V, where we compare and discuss the theoretical and experimental results for the optical transition energies, as a function of well width and temperature, and Sec. VI, with the summary of the main results and conclusions.

II. SAMPLES

The $PbTe/Pb_{1-x}Eu_xTe$ MQW samples were grown on freshly cleaved (111)BaF_2 substrates in a RIBER 32P MBE system equipped with PbTe, Eu, and Te effusion cells.[15] An ion gauge, calibrated with a quartz crystal oscillator, measured the beam flux rates from the effusion cells. The ratio between the Eu and PbTe beam fluxes was used to obtain the nominal Eu content. For optimal growth conditions, the Te flux was two times the one of Eu.

A schematic diagram of the MQW samples is shown in Fig. 1. Before growing the MQW structure proper, a thick (~ 4 μm) $Pb_{1-x}Eu_xTe$ buffer layer (with the same x value as in the barriers) was grown on top of the BaF_2 substrate, in order to accommodate completely the 4.5% lattice mismatch. The growth temperature, for both the buffer and the MQW's, was 300 °C. The PbTe and Te effusion cell shutters always stayed open during the growth process. Opening and closing the Eu shutter controlled the thickness of the barrier and well layers, respectively. The QW growth was repeated 50 times to ensure sufficient infrared optical absorption. *In situ* reflection high-energy electron diffraction (RHEED) at 12 keV was used to monitor the growth process. RHEED intensity oscillations were observed at low temperatures for both PbTe and $Pb_{1-x}Eu_xTe$ growth. Except during the nucleation and coalescence of the $Pb_{1-x}Eu_xTe$ buffer layer, the RHEED pattern showed elongated spots lying on a semicircle, characteristic of an atomically flat surface. Despite the lattice mismatch between $Pb_{1-x}Eu_xTe$ and PbTe layers ($\sim 0.28\%$), the RHEED pattern remained unchanged until the end of the growth.

TABLE I. Data of the $PbTe/Pb_{1-x}Eu_xTe$ MQW samples: period (P), well width (L), parallel strain in the well ($\epsilon_\parallel$), barrier energy gap at 5 K (E_g^b), and Eu content (x), determined from the following empirical expression for the $Pb_{1-x}Eu_xTe$ energy gap $E_g^b(x,T) = 189.7 + 0.48[T(K)^2/T(K) + 29](1 - 7.56x) + 4480x$ meV (Ref. 25).

Sample	P(nm)	L(nm)	$\epsilon_\parallel(10^{-3})$	E_g^b (meV)	x
			1st Series		
M443	58.2	5.3	2.68	498	0.069
M440	62.2	10.4	2.69	490	0.067
M442	67.6	15.6	2.42	501	0.069
M441	72.1	20.6	1.89	488	0.067
			2nd Series		
M457	51.0	2.3	2.32	476	0.064
M462	50.2	4.5	2.20	440	0.056
M461	56.2	9.2	1.85	424	0.052
M460	60.0	14.0	1.87	436	0.055
M456	62.1	17.9	2.01	488	0.067

Two series of samples were produced with slightly different growth conditions. The growth rate, which is determined mainly by the PbTe effusion cell temperature, was the main difference (0.22 nm/s for the first series and 0.38 nm/s for the second). The other growth parameters were kept constant in order to assure sample reproducibility. As a consequence, the average Eu content, which was measured optically (see Table I) was found to be a little bit smaller in the 2nd series. The difference, however, is in the order of the variation in x among the samples inside the series. When discussing the results for the transitions between the lower energy states, which are less sensitive to the barrier height, the two series can in fact be considered as a single uniform series of high-quality $PbTe/Pb_{1-x}Eu_xTe$ MQW samples with $0.05 < x < 0.07$ and varying PbTe well width.

The period (well width plus barrier width) and the strain inside the PbTe layers, for each sample, were determined by high-resolution x-ray diffraction. We have used a Philips X'Pert diffractometer in the triple axis configuration, i.e., a four-crystal Ge (220) monochromator in the primary beam and a Ge (220) channel-cut analyzer immediately before the detector. Figure 2 shows, as an example, the $\omega/2\Theta$ scan of the (222) Bragg diffraction peak for a narrow ($L = 2.3$ nm) and a relatively wide ($L = 17.9$ nm) well samples. Note that the spectra exhibit a very well-resolved satellite peak struc-

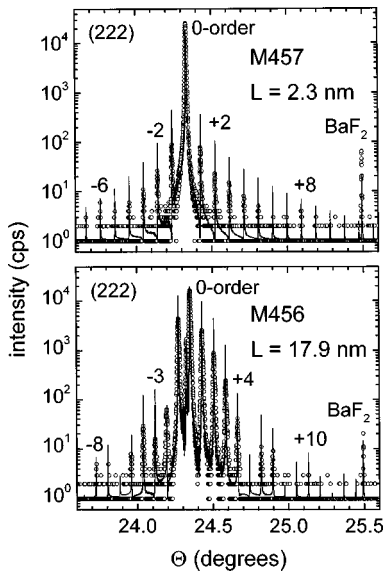

FIG. 2. $\omega/2\Theta$ scan of the (222) Bragg diffraction peak for two PbTe/$Pb_{1-x}Eu_xTe$ MQW samples with different well width L. The solid lines are the calculated spectra that best fit the experimental data (open circles). The spectra exhibit up to the tenth-order satellite peak with full width at half maximum of approximately 25 arc sec, indicating the good structural quality of the grown samples.

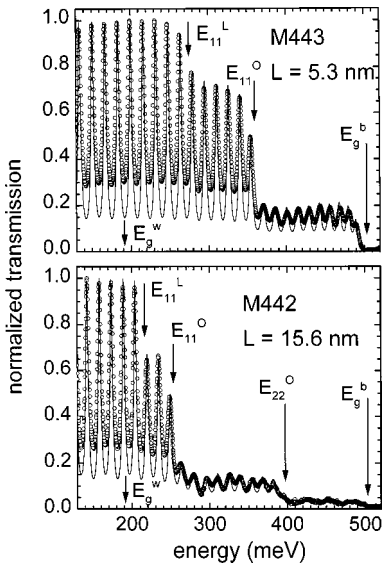

FIG. 3. Infrared optical transmission spectra measured at 5 K, for two PbTe/$Pb_{1-x}Eu_xTe$ MQW samples, with well width $L=5.3$ and 15.6 nm. The solid lines are the results of the simulation, and the circles correspond to the measured data. The arrows indicate the main optical transitions (E_{11}^L, E_{11}^O, and E_{22}^O), obtained from the best-fit procedure, together with the PbTe well (E_g^w) and $Pb_{1-x}Eu_xTe$ barrier (E_g^b) band gaps.

ture showing up to the tenth order. The BaF_2 substrate peak is used as a reference for the Θ scale. The peak corresponding to the $PbEu_{1-x}Te_x$ buffer layer in general overlaps with the zero-order peak of the MQW structure, and is resolved only in the case of wide well samples. The full width at half maximum of the zero-order peak was always approximately 25 arc sec in the $\omega/2\Theta$ direction and three times larger in the ω direction, attesting to the good structural quality of the samples. All satellite peaks exhibited approximately the same width as for the zero-order peak, indicating that sharp interfaces were obtained throughout the MQW structure. The reciprocal space mapping of the (224) asymmetrical reflection indicated that the MQW structure tended to the free-standing condition.[16] With this information, the calculated (222) $\omega/2\Theta$ spectrum (solid line in Fig. 2) was fitted to the measured data, using the in-plane lattice constant ($a^{in\text{-}plane}$) as the main fitting parameter. The tensile parallel strain inside the PbTe well, $\epsilon_\parallel=(a^{in-plane}-a^{\mathrm{PbTe}})/a^{\mathrm{PbTe}}$, where a^{PbTe} is the unstrained lattice constant of PbTe, was then determined with high accuracy, for each sample at room temperature. Details about the structural characterization and strain determination in these MQW samples were published elsewhere.[17]

The main parameters of our samples are listed in Table I. They are the period P, the well width L, the parallel strain in the PbTe well $\epsilon_\parallel$, which were all determined as explained above, and the Eu content x, which was determined from the optically measured $Pb_{1-x}Eu_xTe$ energy gap. The average Eu content obtained (i.e., 0.068 ± 0.001 for the first and 0.059 ± 0.006 for the second series) are only approximately 15% higher than those obtained from the x-ray analysis. Before discussing the optical measurements, it is important to note that, despite the fluctuation in Eu content among the samples, the tensile parallel strain in the well (Table I, 4th column) is found to decrease for increasing well width, due to the increasing strain relaxation.[17]

III. OPTICAL TRANSMISSION MEASUREMENTS

The transmission spectra were measured at temperatures varying from 5 to 300 K, in a Fourier transform infrared spectrophotometer (Perkin Elmer FTIR 1600) with a resolution of 4 cm^{-1} ($\sim$0.5 meV) between 800 and 4500 cm^{-1} (approximately from 100 to 560 meV). A variable temperature He cryostat (Janis supertran-VP) equipped with ZnSe windows was fitted to the Fourier spectrometer measurement chamber. The MQW samples were mounted together with a bare BaF_2 reference substrate in a vertically movable Cu sample holder, with two identical circular holes, inside the cryostat. To avoid extra mechanical strain during cooling down, small clamps, instead of grease or glue, were used to hold the samples. The temperature of the sample holder immersed in a continuous He gas flux was controlled within ±0.1 K, using a Lakeshore 330 auto-tuning controller.

Typical normalized transmission spectra measured at 5 K are shown in Fig. 3. They correspond to the spectra obtained for the samples with $L=5.3$ and 15.6 nm, in the upper and lower panel, respectively. The oscillations are Fabry-Pérot interference fringes caused by the finite thickness of the whole structure (the buffer layer plus the MQW stack). The sharp steplike changes in the transmission intensity are due to the optical absorption corresponding to the interband transitions between the electron and hole confined states in the PbTe QW's. The energies of the main absorbing transitions are indicated. The subscript numbers refer to the subband

indices in the conduction and valence bands and the superscript indicates whether the electron and hole states involved derive from the longitudinal (L) or from the oblique (O) valley (see below). For energies higher than the respective $Pb_{1-x}Eu_xTe$ energy gap (E_g^b), the samples become opaque. In the rest of this section, we explain how we have determined these transition energies as a function of temperature and PbTe well width.

First, it is important to recall that the translation symmetry along the [111] growth direction is broken in PbTe QW's, lifting the fourfold valley degeneracy of the bulk material. The longitudinal valley (along the growth direction) is split from the other three equivalent ones, which are called oblique valleys. Therefore, the optical spectra of these QW's exhibit transitions with different energies, involving different valleys. Since the longitudinal valley has larger electron (and hole) effective mass along the growth direction, the lowest transition energy is usually the first longitudinal transition (as we call the transitions deriving from such a valley).[18] For this same reason, the energy separation between the longitudinal transitions is smaller than that between the oblique ones. On the other hand, due to both the threefold degeneracy and the higher two-dimensional density of free-propagating states along the plane (due, in turn, to the heavier average in-plane effective mass) the oblique transitions are responsible for stronger light absorption. As can be seen in Fig. 3, the clearest absorption steps correspond, in fact, to the first longitudinal transition, which is the absorption edge or threshold, and the strong-absorbing oblique transitions. The other features in the intensity modulation, like the structure between E_{11}^O and E_{22}^O and the tail at high energies in the wide well spectra, are due to the other weaker transitions.

In order to determine accurately the energies of the different optical transitions, we have simulated the transmission spectra using the model calculation introduced by Yuan *et al.*[7] The transition energies are the main parameters in the simulation and are determined from the fitting. First, the absorption coefficient $\alpha(\omega)$ and the refractive index $n(\omega)$ of the $Pb_{1-x}Eu_xTe$ buffer and barrier layers, are determined by fitting, separately, the transmission spectrum of a $Pb_{1-x}Eu_xTe$ epitaxial layer with the same x value as in the MQW structure. The epitaxial layer is treated as a bulk sample with a three-dimensional density of states. Afterwards, for the PbTe layers, a strict two-dimensional response is assumed, where the typical stairlike absorption coefficient, including a level broadening Γ_i for the optical transition energies E_i, can be written as

$$\alpha(\hbar\omega)=\sum_i A_i \frac{1}{\pi}\left[\frac{\pi}{2}+\arctan\left(\frac{\hbar\omega-E_i}{\Gamma_i}\right)\right]\frac{1}{\hbar\omega}, \qquad (1)$$

where A_i stands for the intensity prefactor, proportional to the two-dimensional joint density of states. Finally, the optical transmission through the multilayered structure is calculated using the transfer matrix obtained with properly matching of the electromagnetic fields at all interfaces.[7]

The best fit to the experiments was able to reproduce the main features of the spectra, for every sample and at all temperatures. In Fig. 3, it is plotted with solid lines. As expected, with reasonable values of the parameters Γ_i and A_i, the quality of the fitting is much more sensitive to variations in the energies of the strongly absorbing transitions, as mentioned above, than to variations in the energies of the weaker transitions. We will concentrate our discussion on the strongly absorbing transitions, namely E_{11}^L, E_{11}^O, and E_{22}^O, whose energy positions have been determined with an error never larger than ± 5 meV. The weaker transitions, although playing an important role in the simulation of the transmission spectra, cannot have their transitions determined with such accuracy. One can see in Fig. 4, where specific results of the calculations (see below) are plotted, that between E_{11}^O and E_{22}^O (dashed lines) lie, in general, three longitudinal transitions, and that as the PbTe well width increases, more levels with higher subband indices start to take part in the absorption. This is exactly what was found in the fitting procedure, when trying to reproduce the respective features in the spectra mentioned above. We find that to index the different transitions observed in the transmission spectra of [111] $PbTe/Pb_{1-x}Eu_xTe$ QW's, especially in the case of wide wells, the calculated energy diagram can be particularly useful. Next we explain how this diagram can be easily obtained.

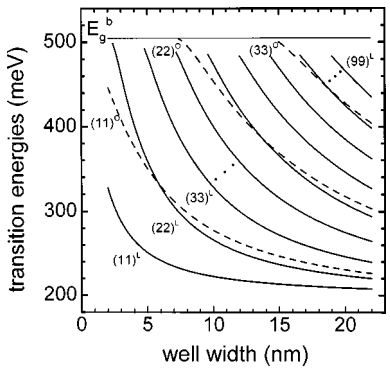

FIG. 4. Optical transition energies for $PbTe/Pb_{0.93}Eu_{0.07}Te$ QW's (at 5 K), as a function of well width, calculated in the envelope-function approximation and the perfect square QW model. The solid (dashed) lines correspond to the energy of the longitudinal (oblique) transitions in an increasing order of subband indices. The straight line represents the top of the barrier (E_g^b).

IV. THEORY

To determine the transition energies, we start from the simple envelope-function model calculation, with analytical solutions, recently proposed to describe the optical transitions in lead-salt QW's.[10] In that work, however, the strain effects had not been considered, in view of the poor knowledge of the strain tensor and of the PbTe deformation potentials. Using the strain, which was measured as a function of well width as discussed in Sec. II, we have included the strain effects and calculated the electric-dipole optical transition energies with different PbTe deformation potentials. This section describes such calculations.

In [111] PbTe epitaxial layers, both quantum size and

strain effects break the fourfold valley degeneracy of the bulk material. The longitudinal valley is split from the three oblique ones. Neglecting valley mixing, the confined states derived from the two kinds of valleys are calculated independently and the electric-dipole transition energies are given by

$$E^i_{nn}=E^w_g+\varepsilon^i_{e,n}+\varepsilon^i_{h,n},\quad i=L(Longitudinal)\ \text{or}\ O(Oblique), \tag{2}$$

where, for example, $\varepsilon^L_{e,n}$ stands for the nth quantized electron energy from the longitudinal valley, $\varepsilon^O_{h,n}$ for the nth quantized hole energy from the oblique valley, and so on. Note that these quantized energies are always positive and measured from the respective band edge. In the case of symmetric square QW's, they are the solutions of the following equations, obtained from a standard plane wave matching, using the Ben Daniel-Duke like boundary conditions:[10]

$$\frac{\chi}{m_b}=\frac{q}{m_w}\tan\left(\frac{qL}{2}\right) \tag{3}$$

and

$$\frac{\chi}{m_b}=-\frac{q}{m_w}\cot\left(\frac{qL}{2}\right), \tag{4}$$

for the even and odd states, respectively, where L is the well width, $q=\pm\sqrt{(2m_w/\hbar^2)\varepsilon}$ and $\chi=\pm\sqrt{(2m_b/\hbar^2)(V-\varepsilon)}$ are the wave vectors in the well (w) and in the barrier (b), respectively. $V=Q(E^b_g-E^w_g)$, for electrons, and $(1-Q)(E^b_g-E^w_g)$, for holes, is the barrier height, where Q is the band-offset parameter. Note that in view of the high PbTe dielectric constant, we neglect the very small band bending.

As already mentioned, the PbTe effective mass along the growth direction m_w depends on the kind of valley. It is m_l or $9m_lm_t/(8m_l+m_t)$ whether the valley is longitudinal or oblique. Within the two-band $\mathbf{k}\cdot\mathbf{p}$ Dimmock model,[19] we have $m_{l(t)}=m_{l(t)}(\varepsilon)=(\hbar^2/2P^2_{l(t)})(\varepsilon+E^w_g)$, where $P_{l(t)}$ is the longitudinal (transverse) momentum interband matrix element. The same is valid for the barrier material effective mass m_b, with only E^b_g in the place of E^w_g (the momentum interband matrix elements are assumed the same in the well and in the barrier). The electron and hole quantized energies, $\varepsilon^i_{e,n}$ and $\varepsilon^i_{h,n}(i=L,O)$, are calculated independently using two different sets of effective momentum matrix elements $\{P^e_l,P^e_t\}$ and $\{P^h_l,P^h_t\}$, which in turn are determined by the bulk band edge effective masses [i.e., $P^{e,h}_{l,t}=(\hbar^2E_g/2m^{e,h}_{l,t})^{1/2}$] which for PbTe, in units of free electron mass and at $T=4$ K, are $m^e_l=0.24$, and $m^e_t=0.024$ for electrons and $m^h_l=0.31$ and $m^h_t=0.022$ for holes.[20] The model we use is therefore an effective two-band $\mathbf{k}\cdot\mathbf{p}$ model.[21]

Let us now consider the strain effects. It is assumed that only the PbTe layers are strained,[22] and that the strain affects only the band gap, leaving the momentum matrix elements constant.[23] The strain correction δE_g to E^w_g depends on the kind of valley and can be written as

$$\delta E^L_g=D_d(2\epsilon_\parallel+\epsilon_\perp)+D_u\epsilon_\perp \tag{5}$$

and

$$\delta E^O_g=D_d(2\epsilon_\parallel+\epsilon_\perp)+D_u(8\epsilon_\parallel+\epsilon_\perp)/9, \tag{6}$$

where $D_d=D^c_d-D^v_d$ and $D_u=D^c_u-D^v_u$ are the differences between conduction and valence-band deformation potentials, and ($\epsilon_\parallel$, $\epsilon_\perp$) are the components of the strain tensor defined with respect to the principle axes of the band extrema (i.e., $\epsilon_\perp\|[111]$, $\epsilon_\parallel\|[1\bar{1}0]$, or $[11\bar{2}]$). Using the elastic constants at 300 K quoted in Ref. 14, we have $\epsilon_\perp=-1.09\epsilon_\parallel$. The only parameters in the calculation of the strain effects are then $\epsilon_\parallel$ and (D_u,D_d). As shown in Sec. II, the room temperature $\epsilon_\parallel$ increases with decreasing well width. In first approximation, and in order to obtain transition energies continuously varying with L, we have used in the calculation the following linear fit $\epsilon_\parallel=(2.63-0.038L[\text{nm}])10^{-3}$ to the data in Table I.

With E^w_g substituted everywhere by $E^w_g+\delta E^i_g(i=L,O)$ the electric-dipole optical transition energies, given in Eq. (2), between quantized electron and hole confined states, are finally obtained from the graphical solution of the Eqs. (3) and (4) for each value of the well width L. The empirical parameters used by the model are $E^b_g(T)$, $E^w_g(T)$, and the PbTe effective masses m_l and m_t at a given temperature (for both electron and holes). The $E^b_g(T)$ used in this work is given in the caption of Table I. For the PbTe temperature-dependent energy gap, we used the following expression obtained from the best fit to the transmission spectra of a thick PbTe/BaF_2 reference sample, measured with the same apparatus described in Sec. III: $E^w_g(T)=190.5+0.45T(K)^2/[T(K)+23]$ meV.

In Fig. 4, as an example, we have plotted the transition energy diagram (i.e., all optical transition energies as a function of the well width) obtained for PbTe/$Pb_{0.93}Eu_{0.07}Te$ QW's at 5 K. A band offset $Q=0.5$ was used.[24] The solid and dashed lines correspond to transitions involving longitudinal and oblique valleys, respectively. The qualitative features of this diagram have already been discussed in Sec. III. Next, we compare our theory with the experimental results.

V. RESULTS AND DISCUSSIONS

A. Well width

We start the discussion with the main results summarized in Fig. 5. There, the obtained energies of the strongly absorbing transitions (E^L_{11}, E^O_{11}, and E^O_{22}) at room and low temperatures are shown as a function of the PbTe well width for all our MQW samples. The theoretical curves, solid and dashed, correspond to the analytical solution of the square well model just described, with Eu concentrations $x=0.05$ and 0.07, respectively. The overall agreement (i.e., for the different transitions, temperatures, and PbTe well width) between the theoretical and experimental results is surprisingly good. We recall that no adjustable parameter is used in the calculation. The model used for the bulk describes quantitatively well both the conduction and valence-band edges. Since the QW confined states were obtained with a standard envelope-function calculation, Fig. 5 shows that such simple effective two-band square well model is, in fact, suitable for describing the quantum confinement effects in PbTe QW's.

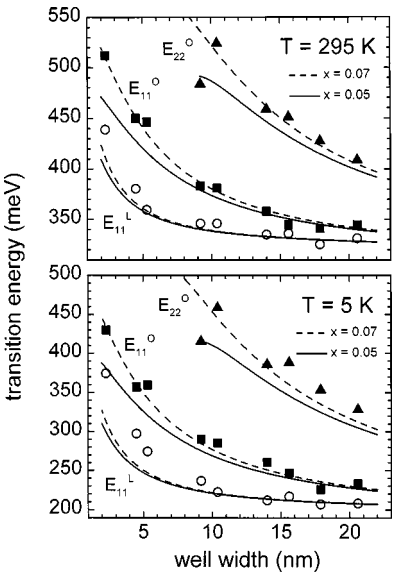

FIG. 5. Strongly absorbing transition energies (E_{11}^{L}, E_{11}^{O}, and E_{22}^{O}) as a function of PbTe well width, obtained from the transmission spectra of our PbTe/$Pb_{1-x}Eu_xTe$ MQW samples at room and low temperatures. The experimental error (± 5 meV) is within the size of the data point. The theoretical curves (solid and dashed) are calculated with the lower ($x=0.05$) and upper ($x=0.07$) limit of Eu content of our series of samples.

The content of Eu determines the barrier height and, for this reason, small fluctuations in x affect only the transition energies close to E_g^b. In fact, in Fig. 5, we see that the results for E_{11}^{L} and E_{11}^{O} in the wide well regime, depend weakly on x. On the other hand, for example, the difference between the measured values for E_{22}^{O} in the case of the samples with $L=9.2$ and 10.4 nm, which have, respectively, $x=0.052$ and 0.067, is quite large and well described by the theory.

Besides the fluctuations in the Eu content, two other main reasons explain the differences seen in Fig. 5 between the theoretical and experimental results: a limit in the applicability of the model and the energy shift due to low-temperature extra strain not included in the calculation. They are connected with the deviations observed at high-transition energies and for very narrow wells. One can see in Fig. 5 that, as the transition energies increase, the theory tends more and more to give values smaller than the measured ones. This is due to the fact that the present $\mathbf{k}\cdot\mathbf{p}$ model for the bulk is less and less accurate as the wave vector (and energy) is increased, and underestimate the energy difference between the real conduction and valence bands. This effect is stronger for the longitudinal valley states, which explains the discrepancies observed in the narrow well limit for the E_{11}^{L} transition. The other problem is the use of the same strain (measured at room temperature) in all calculations. The bigger deviations observed at low temperatures for the narrow well samples, as discussed in more detail below, indicate the buildup of further strain that pushes the measured transition energies further up, away from the theory.

B. Deformation potentials

The strain effects, as discussed in Sec. IV, depend both on the strain tensor and on the deformation potentials. The

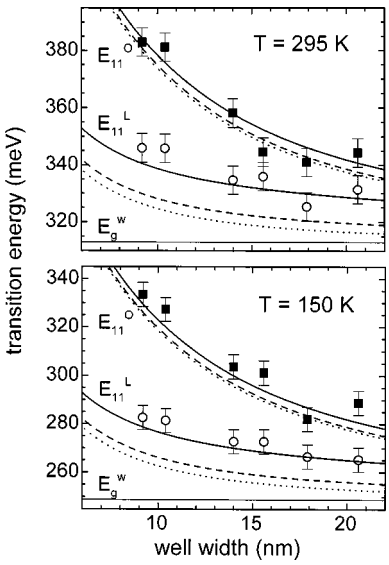

FIG. 6. Comparison, at room temperature and 150 K, between the experimental data for E_{11}^{L} and E_{11}^{O} and the theoretical results obtained with two different sets of PbTe deformation potentials: [$D_d=1.14$ eV and $D_u=-0.55$ eV (Refs. 8 and 23)], represented by the dashed lines, and [$D_d=4.3$ eV and $D_u=-2.8$ eV (Refs. 11 and 12)], given by the solid curves, which practically agree with those obtained using the potentials calculated in the APW framework [$D_d=4.57$ eV and $D_u=-2.17$ eV (Ref. 13)]. The straight line in the bottom of each panel signs the respective PbTe energy gap (E_g^w). The no-strain approximation, dotted lines, is also plotted in order to compare the quantum size and strain effects.

strain was measured at room temperature with high accuracy and here we discuss our choice of PbTe deformation potentials. There is a controversy in the literature about the values of these potentials. After enormous fluctuations found among the first values determined by transport measurements, more precise optical studies lead to values not far from the available first-principles calculations. We have performed the calculation of the optical transition energies using two different sets of deformation potentials. Figure 6 plots the theoretical results, together with the experimental data, at two different temperatures, and in the region of applicability of the model. The dashed curves correspond to calculations using $D_d=1.14$ eV and $D_u=-0.55$ eV, as the ones assumed in Ref. 8, which are similar to values determined by magneto-optical investigations in strained PbTe,[23] whereas the solid lines were obtained using $D_d=4.3$ eV and $D_u=-2.8$ eV,[11,12] which are mean values obtained from shifts in photoluminescence spectra of PbTe thin layers grown on different substrates. These values are very close to the deformation potentials calculated by Ferreira[13] in an augmented plane-wave (APW) framework (i.e., $D_d=4.57$ eV and $D_u=-2.17$ eV). The results without strain ($\epsilon_{\parallel}=0$), given by the dotted lines, are also plotted.

We first note that both the strain corrections and the differences between the results with the two different sets of deformation potentials are of the order of the uncertainty in the determination of the transition energies. Consequently, a precise determination of D_u and D_d is not possible here. Nevertheless, the set of PbTe deformation potentials deter-

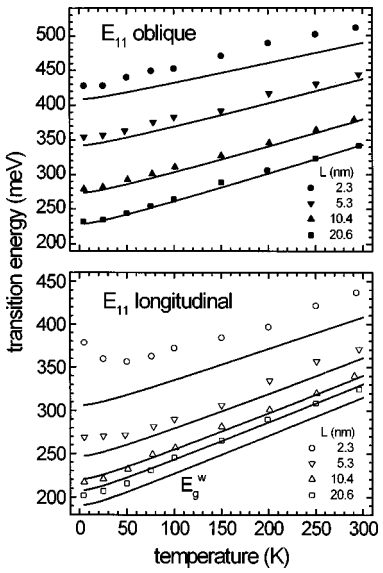

FIG. 7. Temperature dependence of the first longitudinal (lower panel) and first oblique (upper panel) transition energies for four representative samples with different PbTe well width L. For comparison, the PbTe energy gap (E_g^w) is plotted in the lower panel. The theoretical results correspond to the continuous lines and include the correction due to the strain measured at room temperature. Note the increasing blueshift in the longitudinal transition below 100 K for samples with $L<5$ nm.

mined by Valeiko *et al.*[11,12] and calculated by Ferreira[13] leads to a better agreement between the calculated curves and our experimental data at 295 and 150 K. We have used these values throughout the paper. It is also interesting to note that the longitudinal transitions suffer a much larger strain shift when compared to the oblique ones. This result becomes even more evident at lower temperatures, where the thermal strain starts to play a role.

C. Temperature

Our temperature-dependent data can be summarized as done in Fig. 7. In the upper (lower) panel, we have plotted E_{11}^O (E_{11}^L) as a function of temperature, for samples with different PbTe well widths. One can see that, in fact, except at low temperatures, the theory reproduces well the temperature dependence of the transition energies, which is determined mainly by the PbTe energy gap temperature dependence $E_g^w(T)$, plotted in the lower panel. As the transition energy increases (i.e., for narrower wells) the slope tends to decrease a little, as an effect of the nonparabolicity. As already discussed, the difference between theory and experiment seen in these high-energy transitions, which is almost temperature independent, is due to the limitations of the model.

More interesting are the low-temperature deviations observed for the narrow wells in the lower panel of Fig. 7. Instead of decreasing monotonically with decreasing temperature, as in the case of the oblique E_{11}^O level, the E_{11}^L transition, for the samples with $L=2.3$ and 5.3 nm, saturates and starts to increase as the temperature is reduced. An increasing blueshift, seen only in the longitudinal transition energies, is developed during cooling below around 100 K. It competes with the decreasing bulk PbTe energy gap and leads to the minimum observed in E_{11}^L, when the PbTe QW is thinner than approximately 5 nm.

It is known that the mismatch between the thermal expansion coefficient of BaF_2 and PbTe increases considerably at temperatures below near 150 K. Due to the lower thermal expansion coefficient of BaF_2, a tensile strain is built up during the cooldown process. To give a quantitative basis, the total thermal tensile strain would be approximately 1.6×10^{-3} when cooling a thin PbTe layer grown on a BaF_2 substrate from room temperature down to 5 K.[12] In the case of a single PbTe layer thicker than around 2 μm, this thermal strain is expected to be completely relaxed through the dislocations and defects at the BaF_2 interface. Although we have a thick $Pb_{1-x}Eu_xTe$ buffer layer (4 μm) in our samples, our PbTe thin layers are already tensile strained inside the MQW structure by the $Pb_{1-x}Eu_xTe$ barriers. This extra thermal tensile strain may be added to the existing lattice strain in the PbTe wells inside the structure. This phenomenon explains at least qualitatively the above mentioned low-temperature features in the lower panel of Fig. 7. The fact that the blueshift is only observed for the longitudinal transitions, which are much more sensitive to strain effects, reinforces the extra strain explanation, and the reduced effect in the case of wider wells would be due to the respective stronger strain relaxation. In any case, the quantitative description of this effect is outside the scope of this paper. It would require, for instance, the determination of the strain at low temperatures, which is work in progress.

VI. CONCLUSIONS

Summarizing, we have investigated the infrared transmission spectra of a series of high-quality PbTe/$Pb_{1-x}Eu_xTe$ MQW samples grown by MBE. The optical transitions between quantized electron and hole states confined in the PbTe thin layers were determined from the sharp steplike changes in the transmission intensity. The electric-dipole transition energies were calculated by the simple square well model, with analytical solutions within the envelope-function approximation, including the strain corrections, and an overall good agreement was obtained with the measured data. The model was shown to describe well quantitatively these transition energies as a function of well width and temperature, and for all different transitions measured with enough accuracy, namely E_{11}^L, E_{11}^O, and E_{22}^O. The strain inside the PbTe QW's and its effects in the optical spectra were also investigated. We have distinguished the strain energy shift from the quantum confinement, and discussed the values of the PbTe deformation potentials. A blueshift in the energy of the longitudinal transitions was observed during cooling below 100 K, and attributed to the mismatch in the thermal expansion coefficient between the BaF_2 substrate and the PbTe MQW structure. Future measurements of the strain at low temperatures will, however, be necessary before definite conclusions are made.

Finally, the present results demonstrate our satisfactory control of the quantum size effect in these narrow-gap semiconductor QW's. The analytical description of their electronic structure given in this paper is completely transparent and can be of great help in the study of other properties and other PbTe nanostructures. Lead telluride is, for instance, a good candidate material for the new magnetoelectronic or spintronic devices, due to its high-electron mobility and strong spin-orbit interaction. The present model calculation can assist the study of the spin-dependent electron transport in different PbTe nanostructures and devices.

ACKNOWLEDGMENTS

This research has been supported in Brazil by FAPESP (Project Nos. 95/6219-4 and 97/06993-4) and CNPq (Project Nos. 300397/94-1, 301091/95-1, and 300429/97-5). We are very grateful to J.R. Senna for the critical reading of the manuscript.

*Permanent address: Departamento de Física, Universidade Federal de Viçosa, 36751-000 Viçosa- MG, Brazil

[1] D. L. Partin, in *Semiconductors and Semimetals*, edited by R. K. Williams and A. C. Beer (Academic, New York, 1991), Vol. 33, p. 311; D. L. Partin, IEEE J. Quantum Electron. **QE24**, 1716 (1988), and references therein.

[2] G. Bauer, M. Kriechbaum, Z. Shi, and M. Tacke, J. Nonlinear Opt. Phys. Mater. **4**, 283 (1995).

[3] G. Springholz, V. Holy, M. Pinczolits, and G. Bauer, Science **282**, 734 (1998).

[4] G. Grabecki *et al.*, Phys. Rev. B **60**, R5133 (1999).

[5] T. Koga, T. C. Harman, S. B. Cronin, and M. S. Dresselhaus, Phys. Rev. B **60**, 14 286 (1999).

[6] A. Ishida, S. Matsuura, M. Mizuno, and H. Fujiyasu, Appl. Phys. Lett. **51**, 478 (1987).

[7] S. Yuan, G. Springholz, G. Bauer, and M. Kriechbaum, Phys. Rev. B **49**, 5476 (1994).

[8] M. Kriechbaum, K. E. Ambrosh, E. J. Fantner, H. Clemens, and G. Bauer, Phys. Rev. B **30**, 3394 (1984).

[9] M. Kriechbaum, P. Kocevar, H. Pascher, and G. Bauer, IEEE J. Quantum Electron. **24**, 1727 (1988).

[10] E. A. de Andrada e Silva, Phys. Rev. B **60**, 8859 (1999).

[11] M. V. Valeiko, I. I. Zasavitskii, A. V. Matveenko, B. N. Matsonashvili, and Z. A. Rukhadze, Superlattices Microstruct. **9**, 195 (1991).

[12] M. V. Valeiko, K. I. Geiman, I. I. Zasavitskii, A. V. Matveenko, and B. N. Matsonashvili, Fiz. Tverd. Tela (Leningrad), **33**, 1086 (1991) [Sov. Phys. Solid State **33**, 615 (1991)].

[13] L. G. Ferreira, Phys. Rev. **137**, A1601 (1965).

[14] H. Zogg, S. Blunier, A. Fach, C. Maissen, P. Muller, S. Teodoropol, V. Meyer, G. Kostorz, A. Dommann, and T. Richmond, Phys. Rev. B **50**, 10 801 (1994).

[15] P. H. O. Rappl, H. Closs, S. O. Ferreira, E. Abramof, C. Boschetti, P. Motisuke, A. Y. Ueta, and I. N. Bandeira, J. Cryst. Growth **191**, 466 (1998).

[16] S. O. Ferreira, E. Abramof, P. H. O. Rappl, A. Y. Ueta, H. Closs, C. Boschetti, P. Motisuke, and I. N. Bandeira, J. Appl. Phys. **84**, 3650 (1998).

[17] E. Abramof, P. H. O. Rappl, A. Y. Ueta, and P. Motisuke, J. Appl. Phys. **88**, 725 (2000).

[18] In a thick quantum well sample, it can happen that the strain energy shift (which is bigger for the longitudinal transitions, see Sec. V) becomes larger than the quantum size shift, and the lowest transition energy will then be from the oblique instead of from the longitudinal valley (Ref. 11).

[19] See, for instance, J. O. Dimmock, in *The Physics of Semimetals and Narrow Gap Semiconductors*, edited by D. L. Carter and R. T. Bate (Pergamon, New York, 1971), p. 319.

[20] G. Nimtz, *Numerical Data and Functional Relationships in Science and Technology*, edited by K. Hellwege and O. Madelung, Landolt-Börnstein, New Series, Group III, Vol. 17, Part F (Springer-Verlag, Berlin, 1993), pp. 171, 172.

[21] Note that we have neglected the influence of the Eu $4f$ localized states, which are known to modify the fundamental absorption of the $Pb_{1-x}Eu_xTe$ compound with $x>0.07$ [see, for instance, M. Iida, T. Shimizu, H. Enomoto, and H. Ozaki, Jpn. J. Appl. Phys., Part 1 **32**, 4449 (1993)]. Since our samples have x always lower than 0.07 and the main optical transitions investigated here are located below the $Pb_{1-x}Eu_xTe$ energy gap, we expect the $4f$ levels to not affect the values of our calculated transitions.

[22] We neglect the strain in the $Pb_{1-x}Eu_xTe$ barriers, which was found to be one order of magnitude smaller than that in the PbTe wells (Ref. 17).

[23] J. Singleton, E. Kress-Rogers, A. V. Lewis, R. J. Nicholas, E. J. Fantner, G. Bauer, and A. Lopez-Otero, J. Phys. C **19**, 77 (1986).

[24] We point out that the present measurements cannot help in the accurate determination of the band offset in these structures. Due to the almost specular symmetry between the valence and conduction bands in these materials, it was found that most calculated transition energies vary within the experimental error when the band offset varies from 0.2 to 0.8.

[25] S. Yuan, H. Krenn, G. Springholz, Y. Ueta, G. Bauer, and P. J. McCann, Phys. Rev. B **55**, 4607 (1997).